

# Effect of Synthesis Conditions on Textural Properties of Silica MCM-41

Seyed Abbas Sajjadi<sup>1</sup>, Ali Izadbakhsh<sup>1,\*</sup>, Khodabakhsh Niknam<sup>2</sup>

<sup>1</sup> Department of Chemical Engineering, Faculty of Petroleum, Gas, and Petrochemical Engineering, Persian Gulf University, Bushehr, Iran

<sup>2</sup> Department of Chemistry, Faculty of Sciences, Persian Gulf University, Bushehr, Iran

## ARTICLE INFO

### Article history:

Received: April 19, 2016

Accepted: November 8, 2016

### Keywords:

MCM-41

Mesoporous

Nano

Sol Gel

Silica

\* Corresponding author;

E-mail: izadbakhsh@pgu.ac.ir

Tel.: +98 912 54313451

Fax: +98 773 3441495

## ABSTRACT

Several samples of mesoporous silica were prepared via sol-gel chemistry in the presence of CTAB as template with variation of stirring intensity and aging time, ratios of CTAB/SiO<sub>2</sub> and NH<sub>4</sub>OH/H<sub>2</sub>O in synthesis mixture. Effects of aging temperature, hydrothermal treatment and ter-Butanol addition to the synthesis mixture on the textural properties of obtained samples were also studied. Results of XRD, SEM, and N<sub>2</sub> adsorption isotherm analyses showed that particle size and morphology of the mesoporous silica were affected by the synthesis conditions; although, no significant change of the pore size (<5 Å) was observed. Thermal effect on the pore size, unit cell and particle morphology was more pronounced than other parameters. The main morphological variations observed in the synthesized samples were transforming the shape of particles from spherical to larger worm-like particles, the crystallinity of mesoporous structure and intensity of the aggregation. MCM-41 samples of particles size in the range of 50 nm to 1 μm with reduction of aging temperature were obtained. Hydrothermal treatment resulted in the formation of large symmetrical hexagonal shape particle of 500 nm. While stirring intensity led to too smaller particle size, very long wormlike particles (up to 2 μm) were formed by using the ter-butanol in the synthesis.

## 1. Introduction

Research on ordered mesoporous silica materials has received increasing attention after the invention of M41S family at Mobil Company in 1992. These materials have attractive properties including good thermal stability, high surface area with controllable particle morphology and mesopore of about 4 nm. MCM-41 as one of the most widely studied ordered mesoporous silica has been the subject of research in various fields of science and technology from sensors and separation [1] to catalysis [2] and drug delivery [3–5].

Therefore, controlling the formation of this kind of mesoporous to produce crystals of the required particle size and pore system is very important. Attempts to synthesize MCM-41 with controlled pore size started soon after their invention [6,7]; however, most of the investigations have focused on the application of MCM-41 [8–14] and other similar ordered mesoporous materials such as SBA-15 [15–21]. Pore size control is one of the important properties of the ordered mesoporous materials for their application in various fields including catalysis, adsorption, and drug delivery [6,7,22–25].

The influence of water content, silicon source, adding sequence of reactants on pore size, pore shape and product morphology was investigated in [6]. The study showed that the morphology of MCM-41 with uniform particle size and narrow mesopore distribution under the very dilute surfactant solution (~1%) turned into irregular or plate-like aggregates at higher concentrations of the surfactant. The aggregation degree of final products with water content or surfactant concentration was determined. The nature of silica source also significantly affected the morphology and pore size distribution of the products.

Successful enlarging of the pore size of mesoporous silica materials was carried out with larger template species such as the docosyltrimethylammonium chloride [26] in the synthesis of MCM-41 and bulky molecules as micelle swelling agent [27–31] such as mesitylene and tri-isopropyl benzene.

In another study, decane as a swelling agent to enlarge pores of MCM-41 samples was used to study the adsorption and release of bulky biomolecule heparin as a new heparin controlled delivery system [23]. As expected, some mesoporous composites could release heparin in the long term with tuned dosage.

Particle morphology and size is another important property [14,18,32–43] which influences the application of ordered mesoporous silicas, probably most seriously in drug delivery [14]. By using a co-condensation method, functionalized mesoporous silica nanoparticles (MSNs) with a MCM-41 pattern of structures were prepared for the drug delivery application. Highly dispersed MSNs with the surface areas greater than 800 (m<sup>2</sup>/g) and spherical size lower than 50 (nm) was reported [14].

Aqueous colloidal mesostructured silica nanoparticles (CMSS) were prepared by varying the kind and amount of trialkylbenzenes (TAB) and by varying Si sources [37].

When 1,3,5-triisopropylbenzene (TIPB) was used as TAB and tetrapropoxysilane (TPOS) tetramethoxysilane (TMS) was used as a Si source, both the pore size (from 4 nm to 8 nm and above than 10 nm) and particle diameter (from 20 nm to 380 nm) were enlarged. TIPB can enlarge the pore size and particle diameter more than TMB. A dialysis process was used

successfully for the removal of surfactants, TAB and the preparation of CMSS.

In this study, the effect of different parameters such as ter-butanol as cosolvent, concentration of the surfactant and base, aging time and temperature on the final morphology of the mesostructured silica was investigated in the basic synthesis solution. Although many research studies have been conducted on the tuning of morphology of silica MCM-41 material, many of them have dealt with their applications in various fields. To the best of our knowledge, a systematic and comprehensive study of the effects of synthesis conditions on the textural properties of MCM-41 has not been reported previously. Furthermore, the synthesis of MCM-41 wormlike particles of 2  $\mu\text{m}$  by using tertiary alcohol is reported for the first time.

## 2. Experimental

### 2.1. Materials

Hexadecyl tri-methyl ammonium bromide (CTAB  $\geq 99.0\%$ , Acros), solution of ammonium hydroxide (NH<sub>4</sub>OH, 25 wt.%, Merck), tetraethyl orthosilicate (TEOS  $\geq 98.0\%$ , Merck), hydrochloric acid (HCl, 36.5 wt.%, Merck) and ter-butanol (TBA, Merck) were used as received.

### 2.2. Preparation

In a typical synthesis experiment, 0.66 g CTAB was added to the solution of 68.3 ml of NH<sub>4</sub>OH (25 wt.%) in 90 ml of deionized water and stirred for 30 min at the given temperature. In the case of using ter-butanol, the required amount was introduced after the addition of CTAB. 3.11 g of TEOS was added dropwise to the previous mixture and stirred for a determined time. The molar composition of the suspension was TEOS/NH<sub>4</sub>OH/CTAB/H<sub>2</sub>O/TBA = 1.0:32.7:0.120:525:0 (1:a:b:c:d). After washing with deionized water and filtration of the suspension for 3 times, the solid product was dried at 50 °C for 24 h. In order to remove the organic species, the obtained solid calcined in air at 550 °C for 6 h with heating rate of 2.5 °C/min. To investigate the effect of hydrothermal treatment, in one sample the suspension was transferred to a Teflon autoclave kept at 70 °C for 24 h. Table 1 reports starting the composition and other synthesis conditions of the prepared samples.

### 2.3. Characterization

The diffraction patterns were recorded using X-ray diffraction (XRD) with a CuK $\alpha$  ( $\lambda=1.5406 \text{ \AA}$ ) 35 kV radiation (D8 Advance, Bruker, Germany) over the range 1°–6° ( $2\theta$ ) at a speed of 0.01°/minute.

The particle morphology of the obtained samples was analyzed by Fe-SEM images taken from Hitachi S-4160 instrument operating at 20 kV.

The mesostructure of the prepared materials was characterized using a Transmission Electron Microscope (TEM, LEO912-AB, LEO) operating at 100 kV and equipped with a high tilt piece achieving a point-to-point resolution of 0.25 nm.

Also, textural properties of the samples were characterized by nitrogen physisorption analysis at 77 K using a Micromeritics Tristar II 3 setup. The calcined samples were degassed at 623 K for 3 h. The specific surface area

( $S_{\text{BET}}$ ) of the materials was calculated using the BET-method in the relative pressure range between 0.06 and 0.25. The pore-size distribution ( $D_p$ ) and pore volume ( $V_m$ ) were determined from the desorption branches of the isotherms using the BJH method.

Table 1. Synthesis conditions of different samples with yield of synthesis

Sample	a	b	d	Time (h)	Temperature (°C)	Stirring Intensity (rpm)	Hydrothermal
M0 (Reference sample)	103.2	0.121	0	2	55	750	-
M-C/S-0.092	103.2	0.092		2	55	750	-
M-C/S-0.05	103.2	0.05	0	2	55	750	-
M-C/S-0.028	103.2	0.028	0	2	55	750	-
M-N/H-0.232	60.43	0.121	0	2	55	750	-
M-N/H-0.116	30.21	0.121	0	2	55	750	-
M-N/H-0.058	15.1	0.121	0	2	55	750	-
M-Time-1	103.2	0.121	0	1	55	750	-
M-Time-4	103.2	0.121	0	4	55	750	-
M-Time-8	103.2	0.121	0	8	55	750	-
M-Temp-20	103.2	0.121	0	2	20	750	-
M-Temp-40	103.2	0.121	0	2	40	750	-
M-Temp-65	103.2	0.121	0	2	65	750	-
M-Temp-55 -H-70	103.2	0.121	0	2	55	750	24 h at 70 C
M-500rpm	103.2	0.121	0	2	55	500	-
M-250rpm	103.2	0.121	0	2	55	250	-
M-T/H-0.005	103.2	0.121	2	2	55	750	-
M-T/H-0.011	103.2	0.121	4	2	55	750	-
M-T/H-0.023	103.2	0.121	8	2	55	750	-
M-T/H-0.047	103.2	0.121	16	2	55	750	-
M-Opt1	60.43	0.092	0	2	55	500	-
M-Opt2	30.21	0.05	0	1	55	500	-

### 3. Results and Analysis

#### 3.1. Effect of CTAB/SiO<sub>2</sub> ratio

Figure 1 shows XRD patterns of Mesoporous silicas obtained by increasing CTAB in the synthesis mixture. According to XRD patterns, the synthesis with CTAB/SiO<sub>2</sub> ratio of 0.028 did not lead to highly ordered mesoporous silica (MCM-41) as diffraction peaks of planes (110) and (200) at  $2\theta$  more than 4 did not appear. Increasing CTAB/SiO<sub>2</sub> ratio to 0.05 resulted in highly ordered mesoporous silicas, MCM-41. However, a reduction of XRD intensity was observed at the higher CTAB/SiO<sub>2</sub> ratios. XRD data of samples with the highest CTAB/SiO<sub>2</sub> ratio indicate a peak shift to right side in comparison with the sample synthesized with CTAB/SiO<sub>2</sub> ratio of 0.05 (designated as M-C/S-0.05). In other words, XRD data represent unit cell length

which decreases with the CTAB/Silicon ratio.

TEM micrographs given in Fig 2 and 3 prove the larger cross section of particles of sample M-C/S-0.05 in comparison with M-C/S-0.125 which are in agreement with the SEM results. TEM micrographs confirm the hexagonal crystal structure of the sample M-C/S-0.125. Parallel structure of cylindrical mesoporous silica rod is observed in TEM micrograph of sample M-C/S-0.05 given in Figure 3.

According to Figure 4 & 5, SEM images of M-C/S-0.028 particles represent a worm-like shape with a minimum length of 400 nm whereas M-C/S-0.125 particles are more spherical in shape with a minimum size of ca. 100 nm. This observation can be described by a wider distribution of growth rate of mesoporous silicon layers at higher CTAB concentrations resulting in spherical like particles, whereas layers of similar length in less concentrations of CTAB would result in worm-like particles [44]. Furthermore, spherical shape of the particles is a better fit to space in a mixture concentrated with micelles. Higher concentrations of CTAB result in the formation of a larger number of micelles and more hexagonal units growing to smaller final size.

N<sub>2</sub> isotherm adsorption data given in Figure 6 did not show pore size variation with CTAB/SiO<sub>2</sub> ratio indicating constant diameter of micelles at least in the studied range. TEM images of M-C/S-0.05 also showed more interconnected particles which could be related to small macroporosity observed in the N<sub>2</sub> adsorption isotherm.

The reduction of unit cell length with almost constant pore size (Table 2) means that wall thickness of the pores reduces at the higher CTAB concentration.

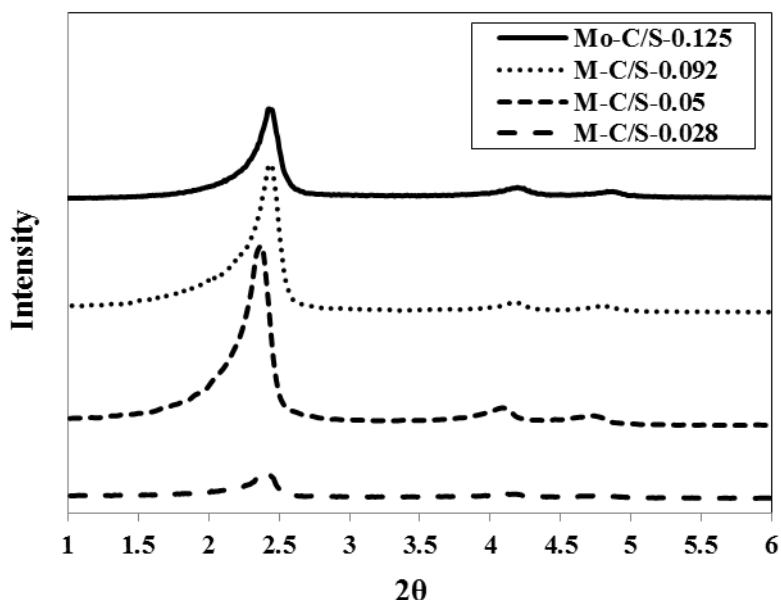


Figure 1. XRD pattern of as-synthesized mesoporous silica with different CTAB/SiO<sub>2</sub> ratios

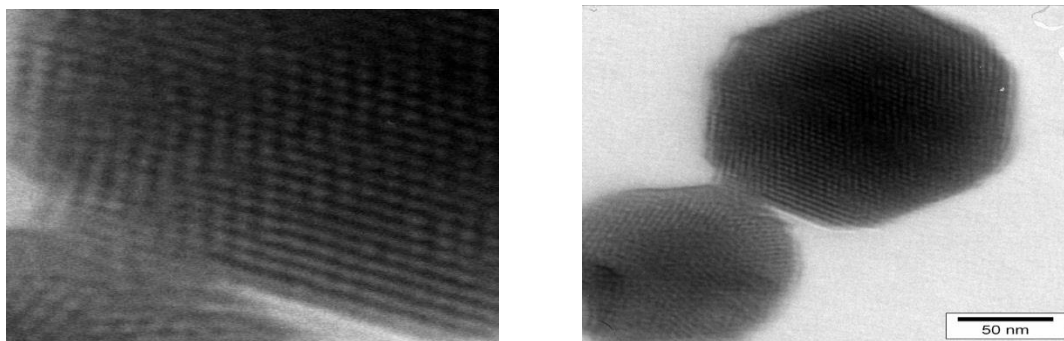


Figure 2. TEM images of Sample M-C/S-0.125

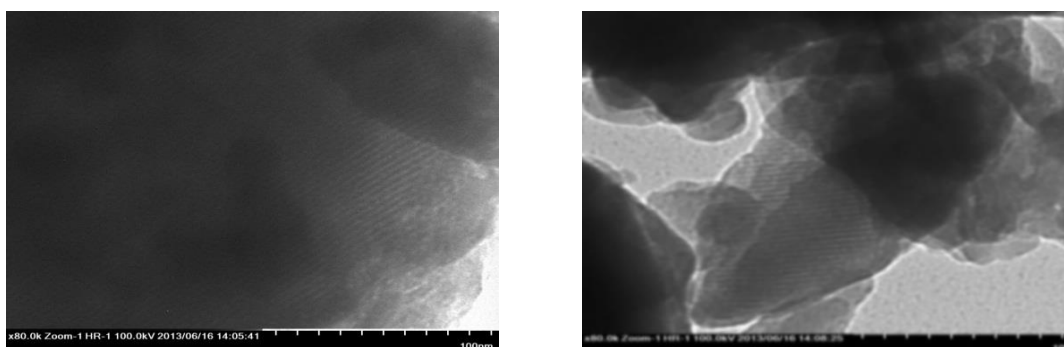


Figure 3. TEM images of Sample M-C/S-0.05

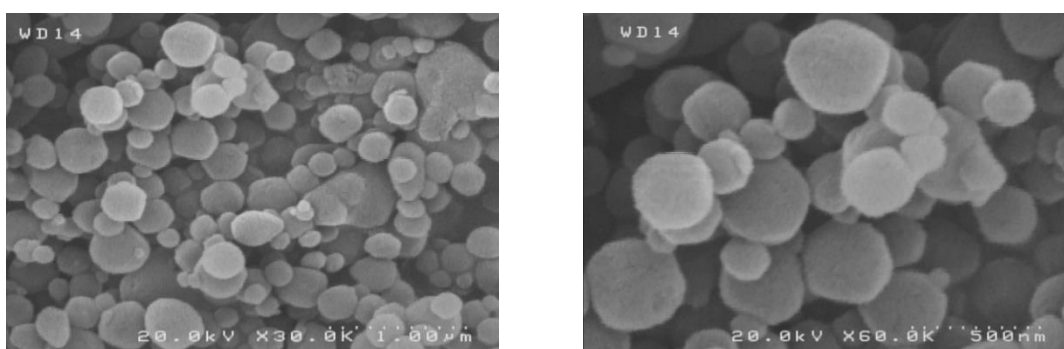


Figure 4. SEM images of Sample M-C/S-0.125

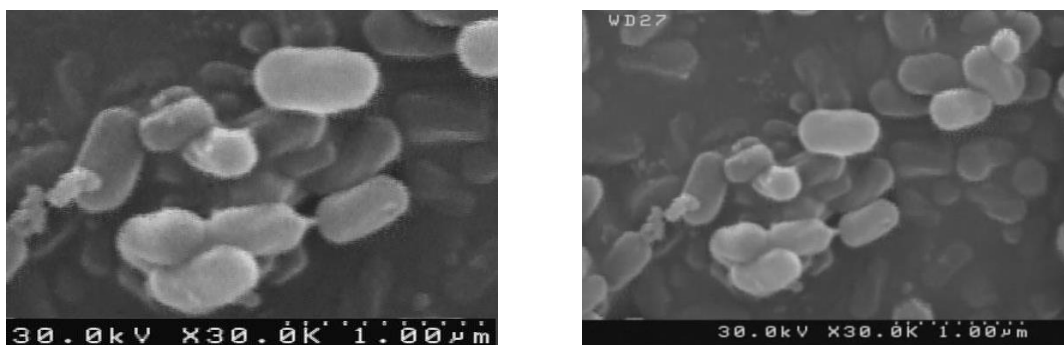
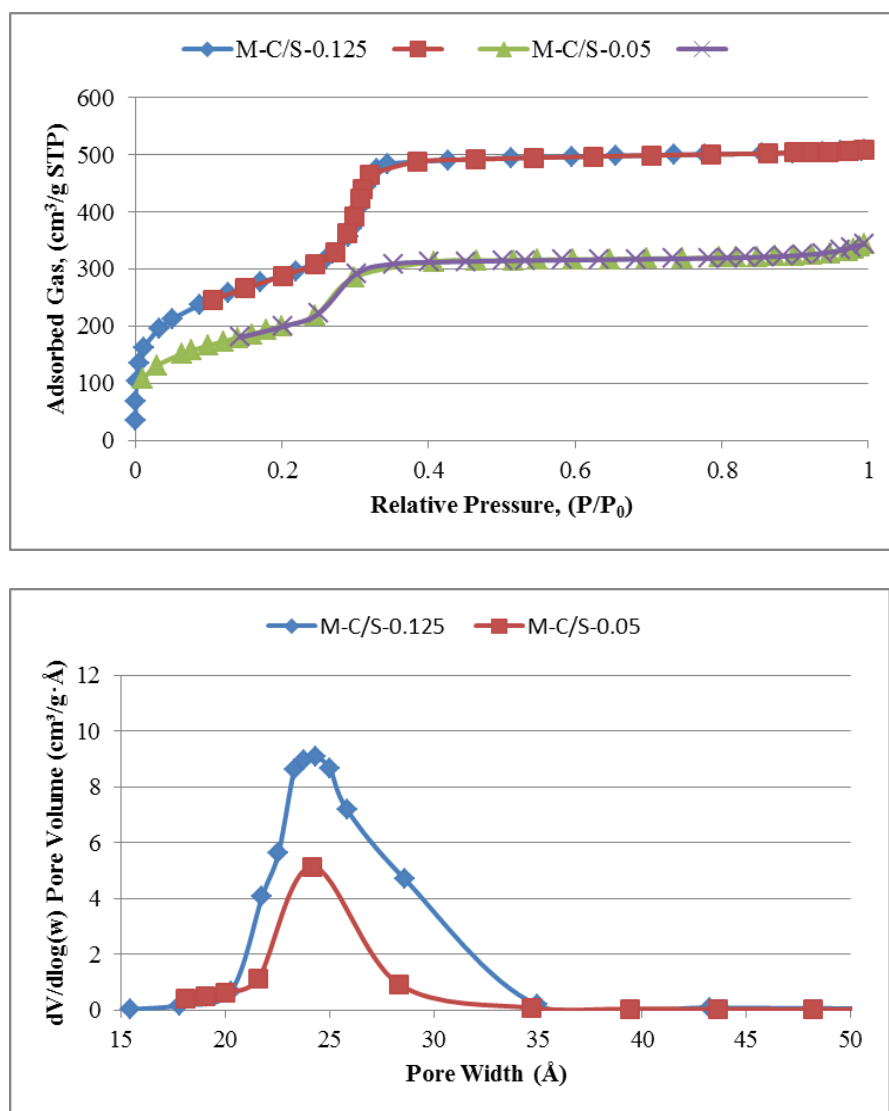


Figure 5. SEM images of Sample M-C/S-0.028

Table 2. Pore structural parameters of the corresponding samples

Sample	Molar ratio of CTAB/SiO <sub>2</sub>	Pore size (°A)	Wall thickness (°A)	Surface area (m <sup>2</sup> /gr)	Pore volume (cm <sup>3</sup> /gr)
M0-C/S-0.125*	0.125	26.0	15.85	1080	0.917
M-C/S-0.05	0.05	24.9	17.92	728	0.507

\*Reference sample

Figure 6. a) N<sub>2</sub> sorption isotherms, b) pore size distribution from Adsorption BJH model of calcined samples synthesized with different CTAB/SiO<sub>2</sub> ratios

### 3.2. Effect of NH<sub>4</sub>OH/H<sub>2</sub>O ratio

Increasing ammonium hydroxide in the synthesis mixture of the mesoporous silica resulted in the less amount of final product which is in agreement with other studies [45]. This observation may be related to the higher

pH of the synthesis mixture. The condensation rate of silica decreases with solution pH after neutral pH [46]. As a result, at lower amounts of  $\text{NH}_4\text{OH}$ , more solid particles are formed as a solid product from synthesis through washing and separation steps. More increase of  $\text{NH}_4\text{OH}$  resulted in the reduced condensation rate of silica and enhanced silica hydrolysis which reduced the obtained solid product. It should be noted that low concentration of  $\text{NH}_4\text{OH}$  has a negative effect on the crystalline hexagonal order of the mesoporous silica as shown in the XRD patterns given in Figure 7. Low hydrolysis with high condensation rate may result in too fast aggregation to establish hexagonal order in all directions.

XRD pattern of samples with different N/H ratios indicates a small peak shift to right side up to the ratio of 0.232 after which the direction of peaks shift reverses. This result implies that  $\text{NH}_4\text{OH}$  amount affects the unit cell dimension of the produced mesoporous silica. Reducing condensation rate with  $\text{NH}_4\text{OH}$  and subsequent reduction of hexagonal silica tubes wall thickness and the reverse trend at the highest N/H ratio shows a dual effect of  $\text{NH}_4\text{OH}$  on the size of the unit cell. A swelling effect on the micelle size may be assumed for  $\text{NH}_4\text{OH}$  after a threshold concentration in the solution.

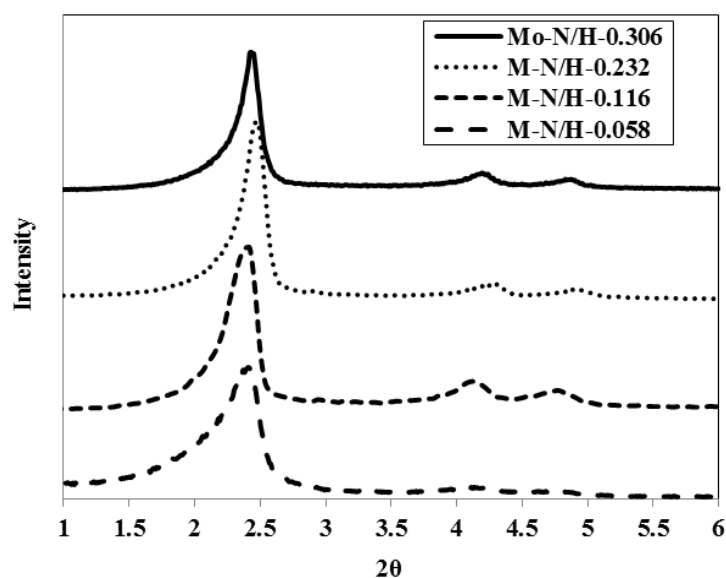


Figure 7. XRD pattern of as-synthesized mesoporous silica with different  $\text{NH}_4\text{OH}/\text{SiO}_2$  ratios

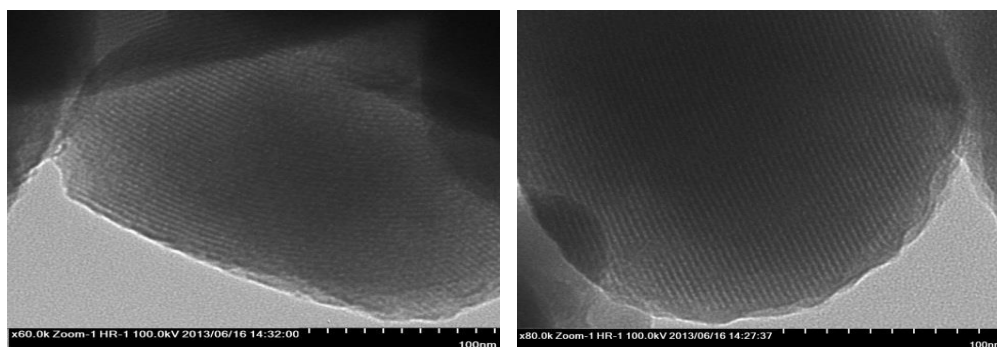


Figure 8. TEM images of Sample M-N/H-0.116

However,  $\text{NH}_4\text{OH}$  amount might influence the particle size of MCM-41 obtained at two other concentrations since signal intensity of their XRD pattern enhances. Higher signal intensity usually correlates with larger crystallite size through Scherrer equation possibly to larger particle at favourable conditions.

Parallel cylindrical structure of the mesoporous silica tubes is observed in TEM micrograph of sample M-N/H-0.116 given in Figure 8. At least one dimension of ca. 200 nm is inferred from TEM micrograph, of M-N/H-0.116 which is larger than particle size of M-N/H-0.306 (Figure 2). This result supports past explanations of XRD size-signal intensity relation.

SEM images of M-N/H-0.116 particles (Figure 9) represent a worm-like shape with a minimum length of 200 nm whereas particles of M-N/H-0.306 (Figure 4) have spherical shape with a minimum size of ca. 100 nm. It seems that less concentration of  $\text{NH}_4\text{OH}$  results in side by side aggregation of smaller building particles giving rise to cylindrical growth. In the condition of higher concentration of  $\text{NH}_4\text{OH}$ , smaller building particles could probably assemble and join together more symmetrically in the presence of sufficient numbers of bridging OH.

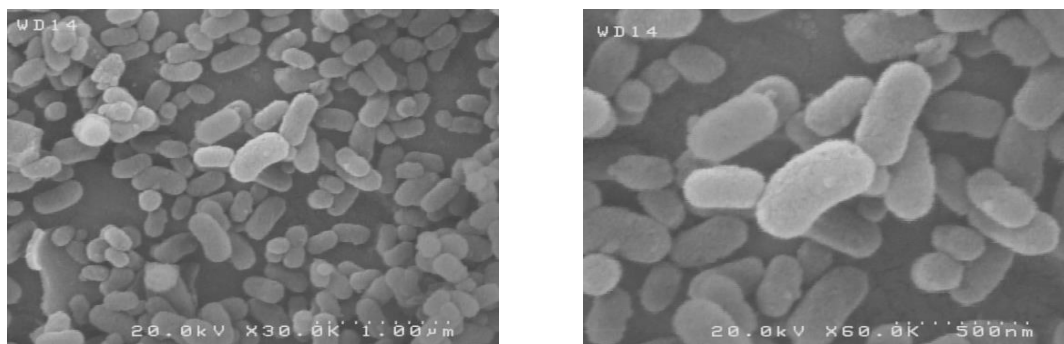


Figure 9. SEM images of Sample M-N/H-0.058

Table 3. Pore structural parameters of the corresponding samples

Sample	Molar ratio of CTAB/SiO <sub>2</sub>	Pore size (°A)	Wall thickness (°A)	Surface area (m <sup>2</sup> /gr)	Pore volume (cm <sup>3</sup> /gr)
M0-N/H-0.306*	0.306	26.0	15.85	1080	0.917
M-N/H-0.116	0.116	24.7	17.5	960	0.676

\*Reference sample

$\text{N}_2$  Adsorption isotherm of M-N/H-0.116 given in Figure 10 shows typical shape of mesoporous materials with a hysteresis loop formed in the middle of  $\text{N}_2$  pressure range. BJH pore size distribution does not indicate any significant changes in the pore size (Table 3) between samples M-N/H-0.116 and M-N/H-0.306 (M-C/S-0.05). It means that the amount of  $\text{NH}_4\text{OH}$  has no effect on the pore size. Although CTAB amount used in the synthesis of the above-mentioned samples are different, no effect on the pore size of products was observed in the previous section.

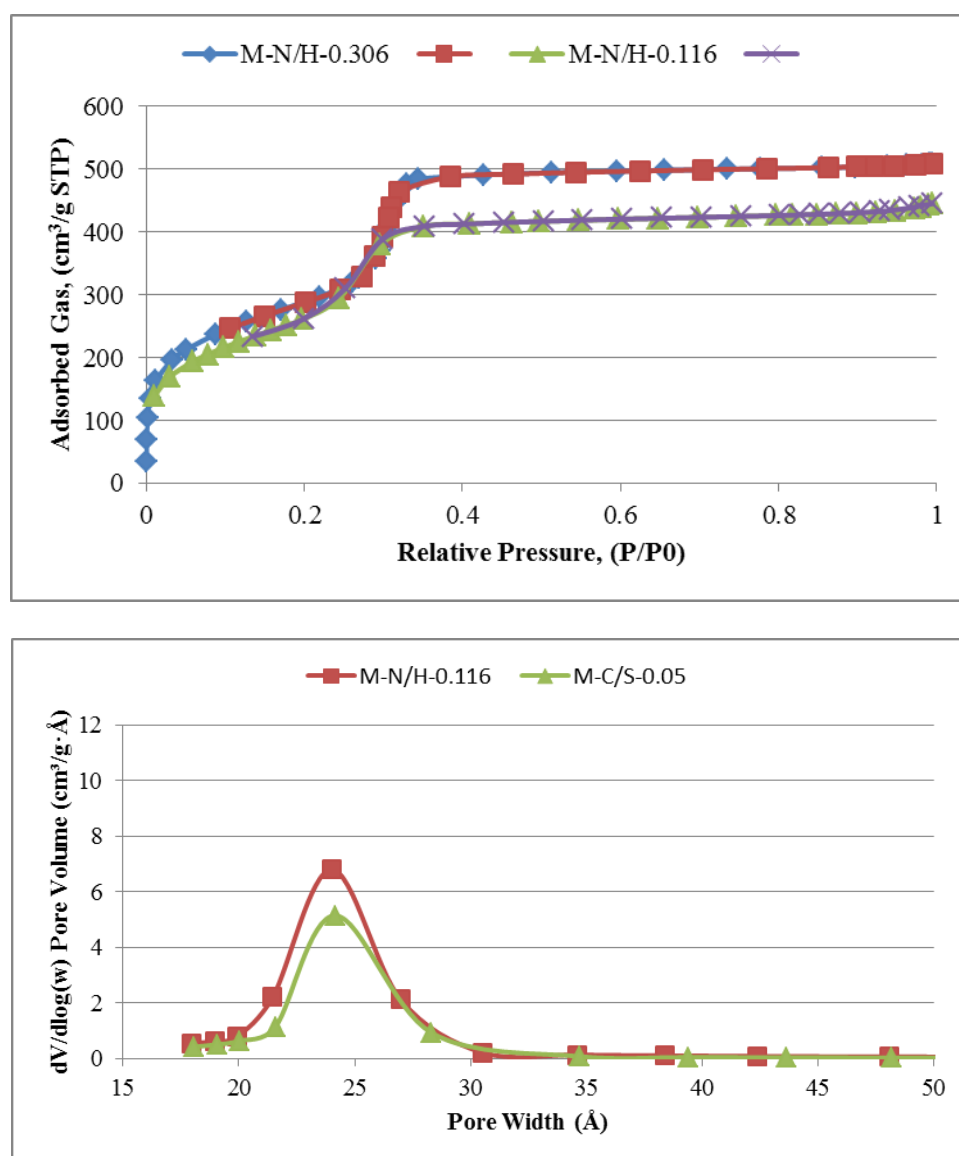


Figure 10. a) N<sub>2</sub> sorption isotherms, b) pore size distribution from Adsorption BJH model of calcined samples synthesized with different NH<sub>4</sub>OH/H<sub>2</sub>O ratios

### 3.3. Effect of Aging Time

According to XRD spectra given in Figure 11, longer aging time (i.e. time of reaction after the introduction of all species) has a significant effect on unit cell of the obtained mesoporous silica as it varied from 41.3 to 42.7. Hexagonal order of the mesoporous silica is formed in the short time of 1h. These observations all indicate that silica tube wall becomes thicker with time while hexagonal assembly of silica tubes has already been established. Comparing SEM images of the sample obtained after 8 h of aging, given in Figure 12, with SEM images of the reference sample (aging time of 2h) given in Figure 4, it can be inferred that particle size of the mesoporous silica increases with aging time. Also ca has the minimum size of the particles (i.e. 500 nm) in the images of Figure 12. Longer aging time provides more time for the aggregation of grains to form larger product particles.

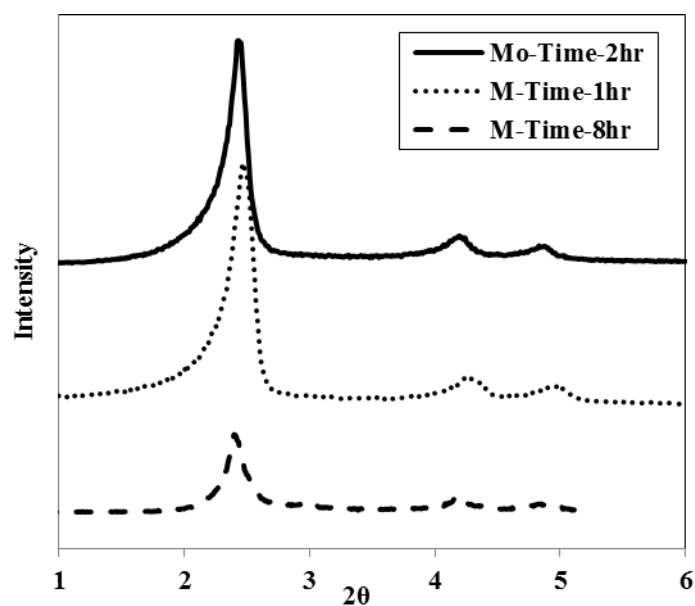


Figure 11. XRD pattern of as-synthesized mesoporous silica obtained at different aging times

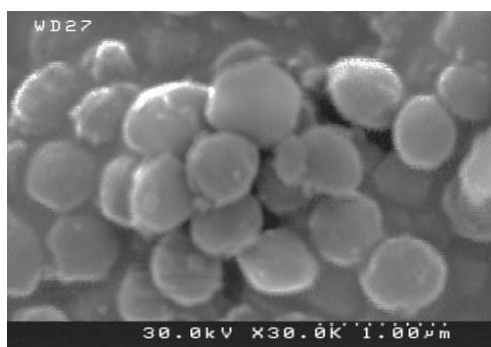


Figure 12. SEM images of Sample M-Time-8h

### 3.4. Effect of Aging Temperature

XRD spectra given in Figure 13 show higher aging temperature (i.e. temperature of mixture after the introduction of all species). It favours mesoporous structure with larger unit cell size and higher hexagonal order. Unit cell size increases with aging temperature by ca. 3 Å.

Another noteworthy observation in the XRD spectra is the intensification of reflections of plane (200) and (110) the sample prepared with hydrothermal treatment at 70 °C.

N<sub>2</sub> sorption data reported in Table 4 indicates that pore size increases with aging temperature from 21 to 25 Å at the expense of wall thickness of silica tubes. It may be concluded that the same concentration of CTAB leads to larger micelles at the higher aging temperatures.

SEM images of sample obtained at the aging temperature of 20 °C shows shapeless large particles of ca. 1 μm size for the shortest dimension. The lower temperature of mixture enhances grain aggregation to larger particles since the process of aggregation is thermodynamically favourable at lower temperatures. Parallel lines in TEM micrograph in Figure 14 confirm the porous structure of the sample M-Temp-20. Species with hollow structure seen in SEM images of

Figure 15 could be responsible for less intensity seen in XRD pattern of sample M-Temp-20.

Hydrothermal treatment at 70 °C for 24 h resulted in mono dispersed particles of nearly hexagonal morphology as seen in SEM graphs given in Figure 16. Particle size increases to at least 500 nm with the applied hydrothermal treatment whereas in the absence of hydrothermal step the particle size reduces to the minimum of 100 nm (M-C/S-0.125). Regarding aging effect on the particle size, the effect of hydrothermal treatment on the particle size may be related to the duration length of this step. The thermal part could influence the pore size of the silica tubes and probably leads to better geometrical order of the hexagonal shape particles.

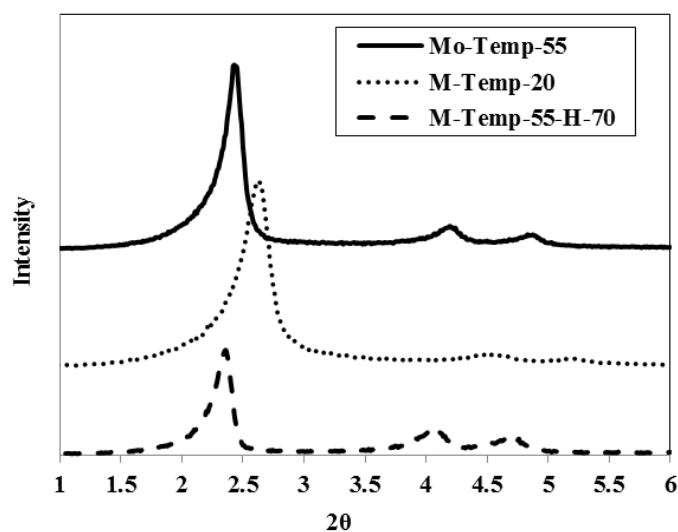


Figure 13. XRD pattern of as-synthesized mesoporous silica obtained at different aging temperatures

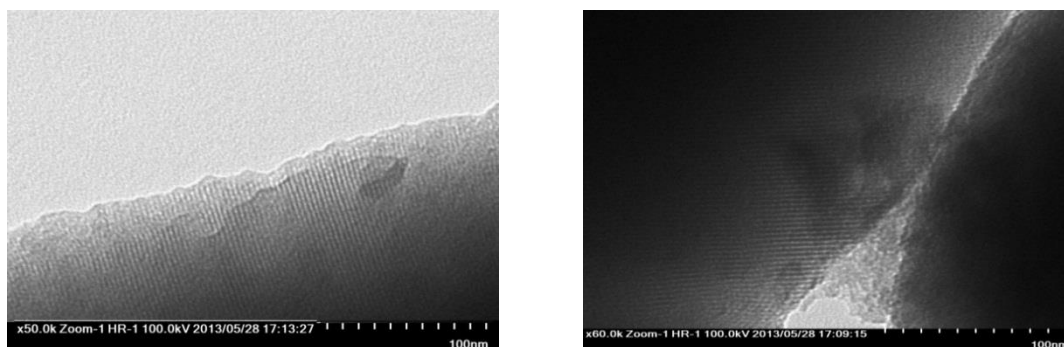


Figure 14. TEM images of Sample M-Temp-20

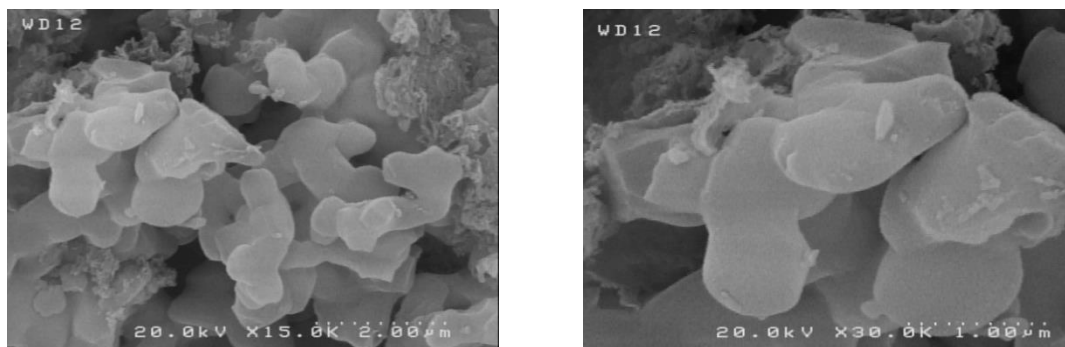


Figure 15. SEM images of Sample M-Temp-20

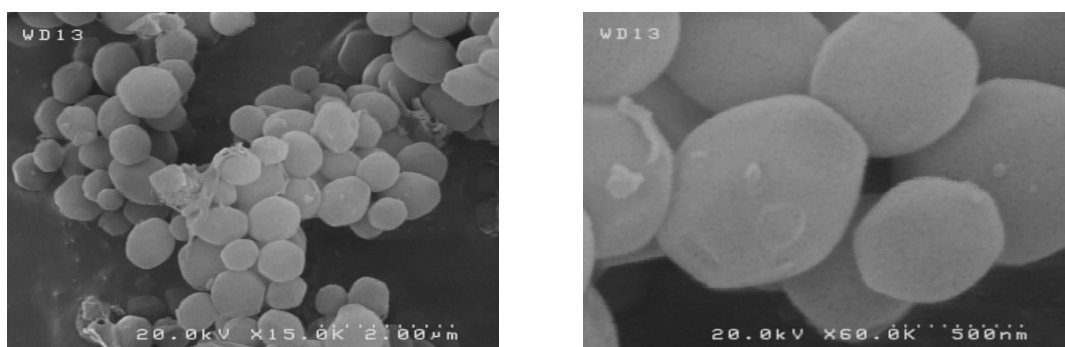


Figure 16. SEM images of Sample M-Temp-55-H-70

Table 4. Pore structural parameters of samples synthesized with different aging temperatures

Sample	Temperature (°C)	Pore size (°A)	Wall thickness (Å)	surface area (m <sup>2</sup> /gr)	Pore volume (cm <sup>3</sup> /gr)
M0-Temp-55*	55	26	15.85	1080	0.917
M-Temp-20	20	21.5	17.1	986	0.411

\*Reference sample

### 3.5. Effect of Stirring Intensity

XRD spectra of samples obtained at different stirring rate given in Figure 18 show no significant peak shift and hexagonal order of MCM-41 is confirmed in all samples with the presence of two relevant reflections in  $2\theta$  range of 4 to 5°. TEM micrographs of sample M-500rpm show typical image of MCM-41 (Figure 19). SEM images of sample M-500 in Figure 20 indicate particle size of 300 to 500 nm which are larger than particles of 100 to 250 nm can be obtained at the stirring speed of 750 rpm. Formation of smaller particles at the higher stirring rate is a known effect in particle growth in liquid phase explained by fluid shear stress exerted on the external surface of the particle. According to BJH, pore size distribution in Figure 21, a considerable contraction of pore size with increasing stirring rate can be observed (Table 5).

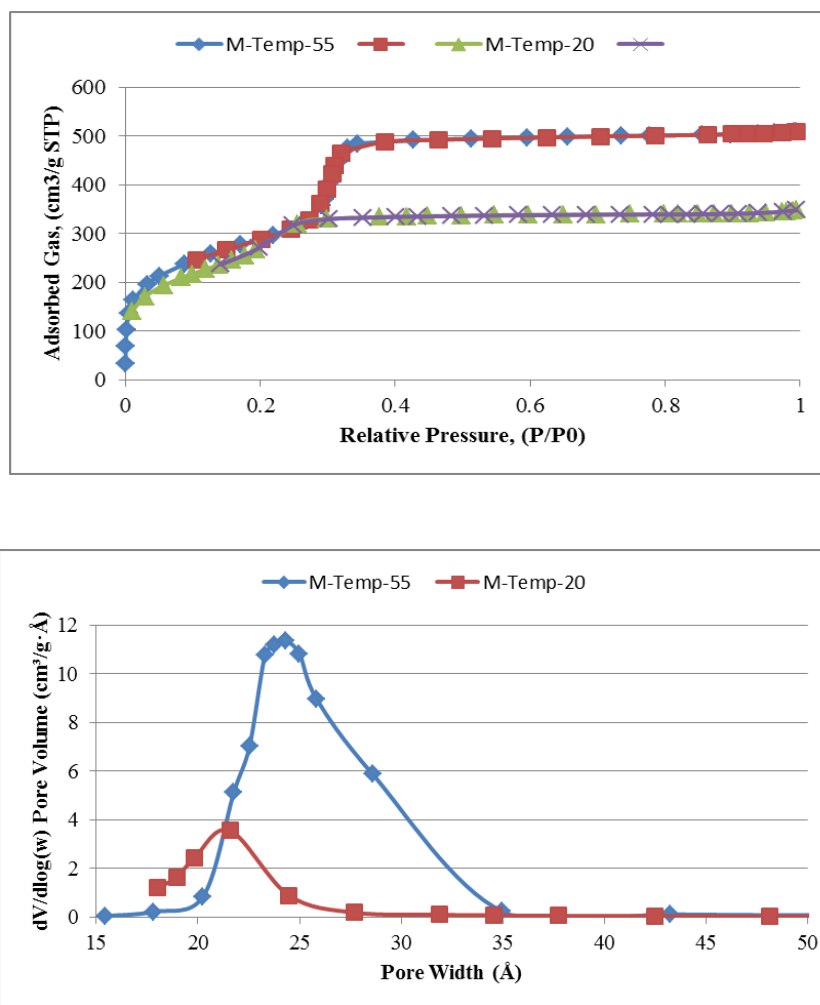


Figure 17. a) N<sub>2</sub> sorption isotherms, b) pore size distribution from Adsorption BJH model of calcined samples synthesized with different aging temperatures

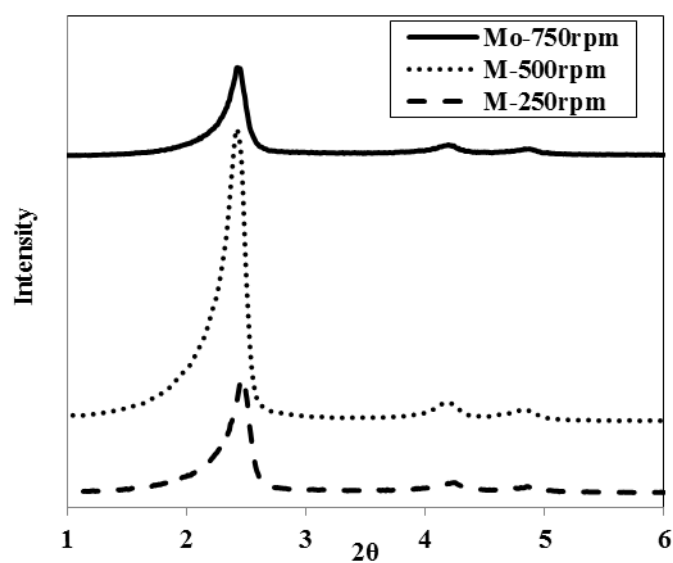


Figure 18. XRD pattern of as-synthesized mesoporous silica obtained at different stirring intensities

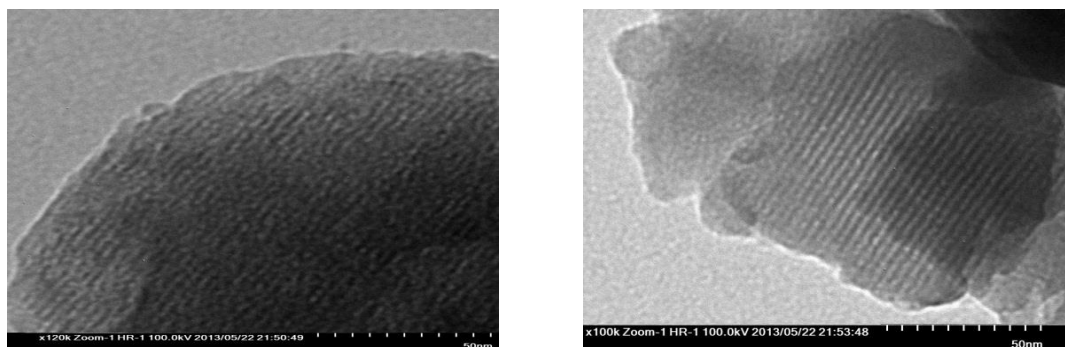


Figure 19. TEM images of Sample M-500rpm

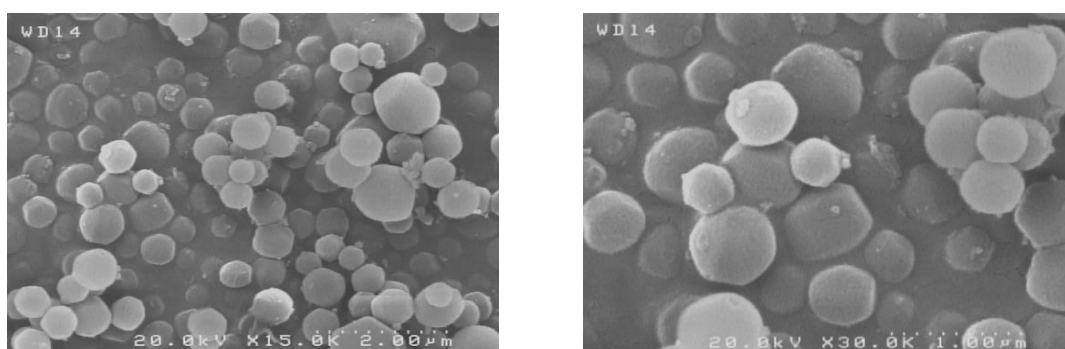


Figure 20. SEM images of Sample M-500rpm

Table 5. Pore structural parameters of samples synthesized with different stirring rates

Sample	Stirring rate (rpm)	Pore size (°Å)	Wall thickness (Å)	surface area (m <sup>2</sup> /gr)	Pore volume (cm <sup>3</sup> /gr)
M0-750rpm*	750	26	15.85	1080	0.917
M-500rpm	500	28.1	14.0	972	0.804

\*Reference sample

### 3.6. Effect of ter-Butanol Addition

XRD pattern data, given in Figure 22, confirm hexagonal order of the prepared mesoporous silica MCM-41 at all ratios of ter-butanol as three standard reflections appeared in the expected  $2\theta$ .

Crystallographic data reported in Table 6 indicate a decrease of unit cell followed by an increase with ter-butanol/H<sub>2</sub>O ratio in the synthesis mixture. The reason for initial contraction of unit cell with ter-butanol addition to synthesis mixture is not clear. However, the consumption of a minor amount of CTAB with ter-butanol in the formation of inactive new micellar system for silica condensation and the contraction of normal micellar system with the remaining CTAB may be a probable reason for this observation. Subsequent unit cell enlargement can be attributed to the swelling effect of ter-butanol on the micelles.

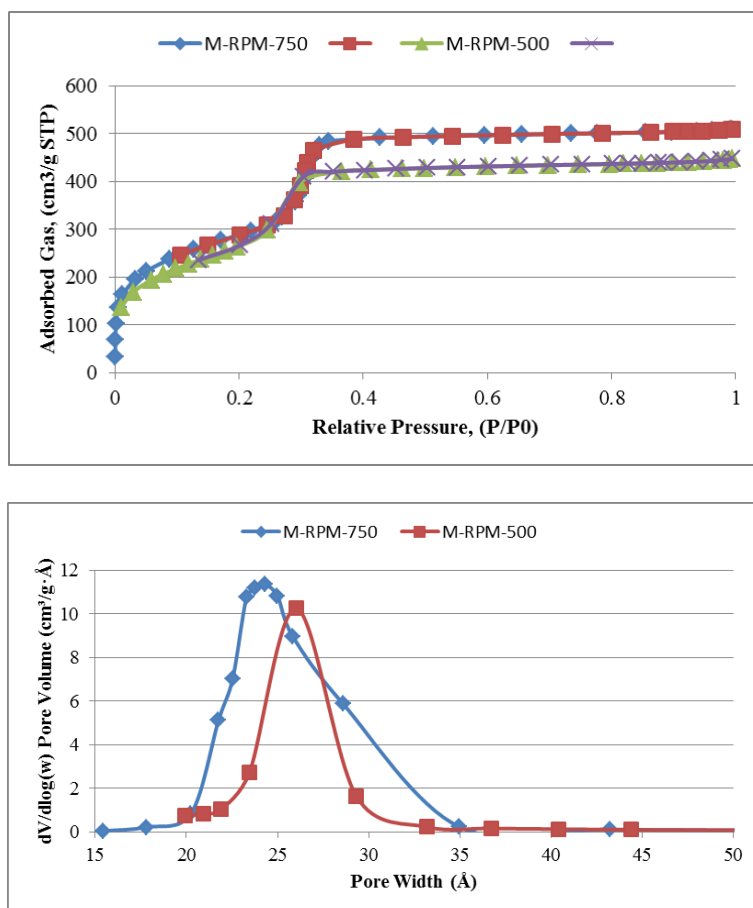


Figure 21. a) N<sub>2</sub> sorption isotherms, b) pore size distribution from Adsorption BJH model of calcined samples synthesized with different stirring rates

SEM image of sample M-T/H-0.011 in Figure 23 indicates the increase of particle size to the range of 1  $\mu\text{m}$  with a wormlike shape. The particle size increase indicates enhancement of condensation/agglomeration rates which can be attributed to the co-solvent role of the ter-butanol.

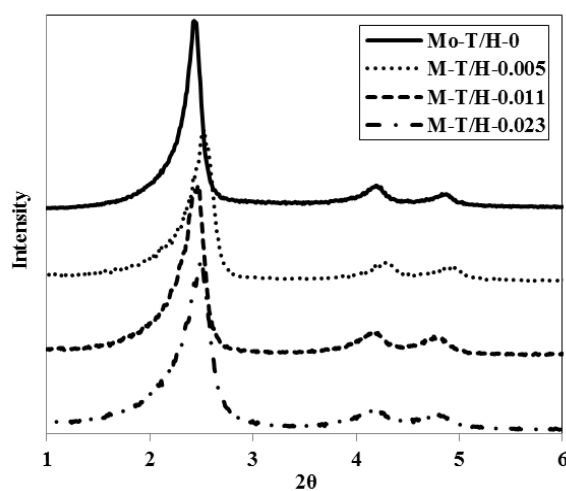


Figure 22. XRD pattern of as-synthesized mesoporous silica obtained at different ter-Butanol ratios

Table 6. Angle of reflection of crystallography planes and unit cell dimension of mesoporous silica prepared with different ter-Butanol ratios

Sample	TBA/H <sub>2</sub> O	2 $\theta$ (100)	Intensity (100)	a <sub>0</sub> (Å)
M0-T/H-0.0*	0	2.43	6300	41.85
M-T/H-0.005	5.94e-3	2.53	5012	40.34
M-T/H-0.011	11.88e-3	2.47	5821	41.28
M-T/H-0.023	23.76e-3	2.50	5791	40.80

\*Reference sample

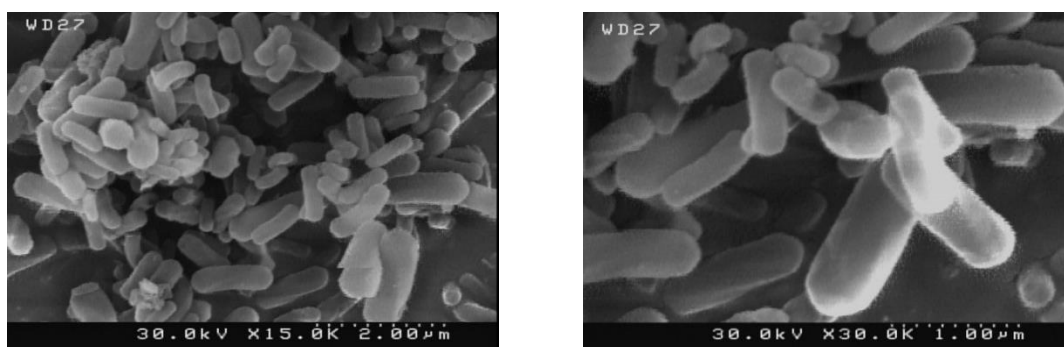


Figure 23. SEM graph of sample M-T/H-0.011

### 3.7. Optimum samples

Results of studies on the influence of different synthesis parameters on the pore size, morphology, hexagonal order and particle size of the prepared ordered mesoporous silicas suggest two selected sets of synthesis parameters to intensify XRD signal intensity (and higher crystallinity) of reflection of plane (100). Synthesis conditions of samples designated as M-Opt1 and M-Opt2 have been given in Table 7.

XRD results in Figure 24 show stronger reflection of plane (100) in M-Opt1 and a peak shift to smaller  $2\theta$  for M-Opt2. More uniform pore wall of M-Opt1 can be inferred by comparing TEM micrographs in Figure 25 and 26, respectively. The interesting TEM image of plane normal to silica tubes centreline given in Figure 26 shows hexagonal arrangement of the silica tubes bundle.

TEM micrograph of sample M-Opt2 (Figure 26, left) shows large mesoporosity as cavities of 10 to 40 nm. Hence, it can be deduced that less amount of NH<sub>4</sub>OH resulted in enhanced macro porosity formation in the prepared samples.

SEM images of M-Opt2 in Figure 27 shows worm-like particles of 150x250 nm<sup>2</sup> which are formed by grains as large as 50 nm. The particles in the reference sample are larger and more spherical.

N<sub>2</sub> adsorption isotherm of sample M-Opt1 and M-Opt2 in Figure 28 shows macro porosity formation, especially in the latter case. SEM images (Figure 4) of reference sample indicate smoother external surface which agrees with its smooth N<sub>2</sub> adsorption curve near the saturation point (P/P<sub>0</sub> ≈ 1).

Table 7. Synthesis conditions of samples designated as optimum samples

Sample	Molar ratio CTAB/SiO <sub>2</sub>	Molar Ratio NH <sub>4</sub> OH/H <sub>2</sub> O	Reaction time (hr)	Temperature (°C)	Stirring rate (rpm)	Hydrothermal
M-Opt1	0.092	0.232	2	55	500	-
M-Opt2	0.05	0.116	1	55	500	-

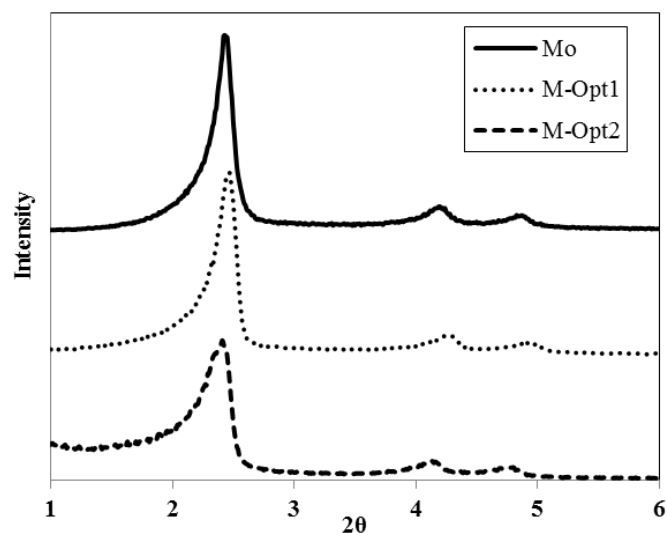


Figure 24. XRD pattern of as-synthesized mesoporous silica obtained at the optimum conditions

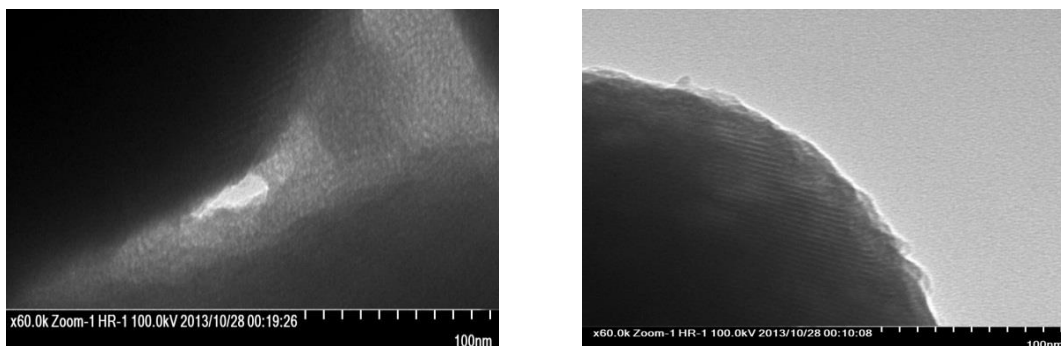


Figure 25. TEM images of Sample M-Opt1

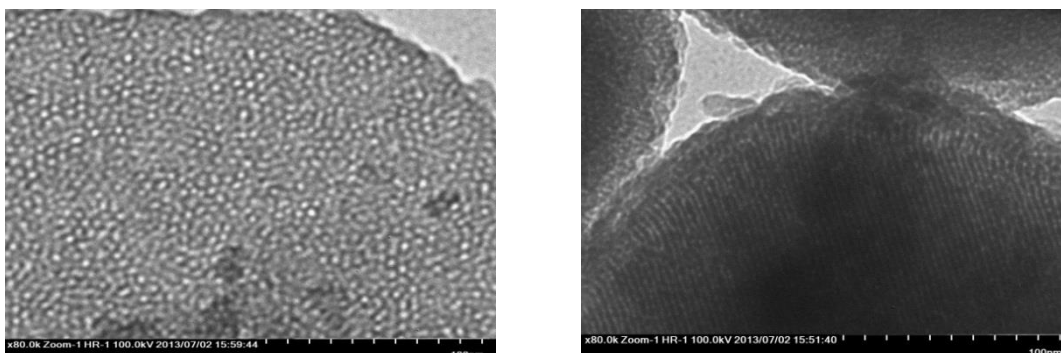


Figure 26. TEM images of Sample M-Opt2

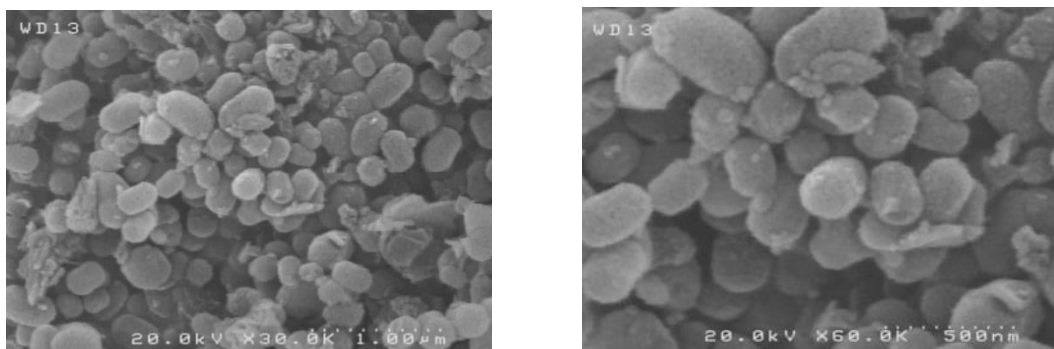


Figure 27- SEM images of Sample M-Opt2

Table 8. Pore structural parameters of samples synthesized at the optimum conditions

Samples	Pore size (°A)	Wall thickness (°A)	Surface area (m <sup>2</sup> /gr)	Pore volume (cm <sup>3</sup> /gr)
M0*	26	15.85	1080	0.917
M-Opt1	25.0	16.25	874	0.636
M-Opt2	26.5	15.9	784	0.759

\*Reference sample

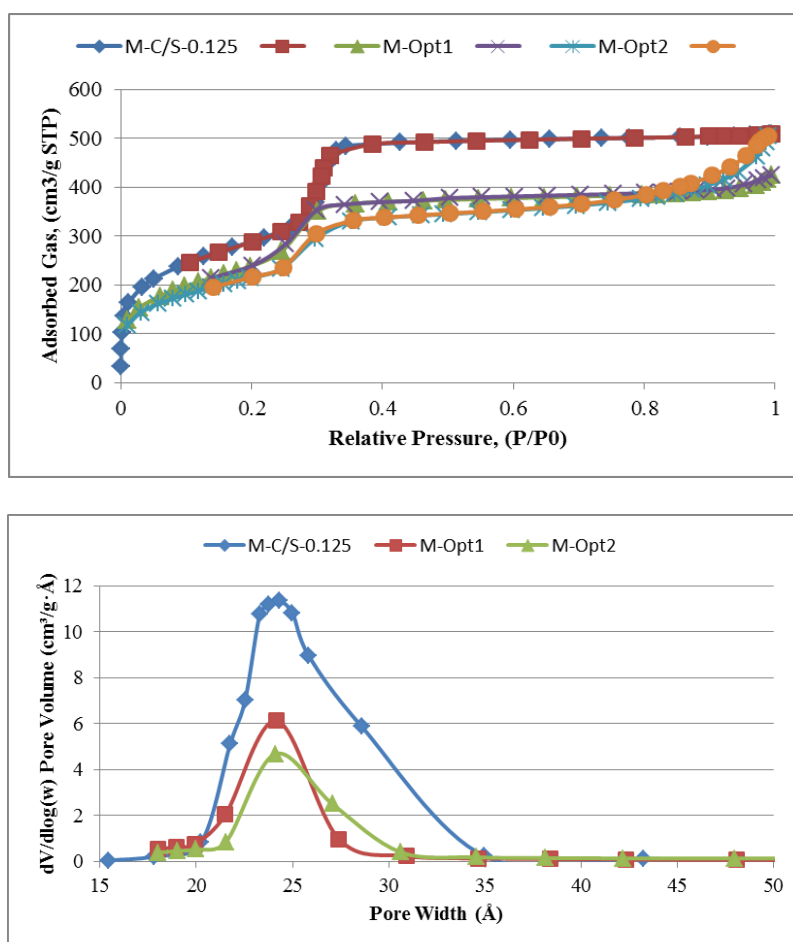


Figure 28. a) N<sub>2</sub> sorption isotherms, b) pore size distribution from Adsorption BJH model of calcined samples obtained at the optimum conditions

#### 4. Conclusions

Increasing template in the synthesis of MCM-41 showed several effects including particle size decrease, change from worm-shape to spherical, and enhancing hexagonal order. Also, no significant influence on the pore size was observed.

More mesoporous silica with the spherical particle instead of worm-shape was obtained by increasing ammonium hydroxide in the synthesis. Particle size reduction was observed at higher  $\text{NH}_4\text{OH}/\text{SiO}_2$  ratios. Low concentration of  $\text{NH}_4\text{OH}$  had a negative effect on the crystalline hexagonal order of the mesoporous silica. No significant influence on the pore size was observed as well.

Longer aging time provides more time for the aggregation of grains to form larger product particles ( $> 500$  nm). Hexagonal order of MCM-41 is formed after 1h of aging time

Thermal effect on the pore size, unit cell and particle morphology was more pronounced than other parameters. The size of pore ( $\approx 5$  Å) and subsequently unit cell increases due to micelle enlargement with temperature. Larger particles ( $> 1$  μm) are formed at lower temperature due to the enhanced aggregation

Using hydrothermal treatment results in the formation of hexagonal-shape large ( $> 500$  nm) particles with the increased size of the pores and the unit cell.

Stirring rate adversely influenced size of the particles (200-250 nm at 250 rpm) and the pore size (2 Å at 250 rpm) of the mesoporous silica. The spherical shape remained unvaried.

Size of the formed wormlike particle ( $>1$  μm) of MCM-41 increased with ter-Butanol which indicates enhancement of the condensation/agglomeration rates due to co-solvent role of ter-Butanol.

Results of the characterization analysis of the sample prepared at lower CTAB/ $\text{SiO}_2$  ratio, less amount of  $\text{NH}_4\text{OH}$ , and higher stirring rate indicated formation of MCM-41 particles with smaller size. Sample of larger particles with the reduced crystallinity was obtained at the lowest amount of  $\text{NH}_4\text{OH}$  and short aging time.

#### Acknowledgment

The study was financially supported by National Gas Company in Bushehr province and Persian Gulf Science and Technology development Center.

#### References

- [1] K. K. Unger, D. Kumar, M. Grün, G. Büchel, S. Lüdtkke, T. Adam, *et al.*, "Synthesis of spherical porous silicas in the micron and submicron size range: challenges and opportunities for miniaturized high-resolution chromatographic and electrokinetic separations," *Journal of Chromatography A*, vol. 892, pp. 47-55, 2000.
- [2] M. Grün, I. Lauer, and K. K. Unger, "The synthesis of micrometer- and submicrometer-size spheres of ordered mesoporous oxide MCM-41," *Advanced Materials*, vol. 9, pp. 254-257, 1997.
- [3] A. Popat, S. B. Hartono, F. Stahr, J. Liu, S. Z. Qiao, and G. Qing (Max) Lu, "Mesoporous silica nanoparticles for bioadsorption, enzyme immobilisation, and delivery carriers," *Nanoscale*, vol. 3, pp. 2801-2818, 2011.
- [4] L. Wang, W. Zhao, and W. Tan, "Bioconjugated silica nanoparticles: Development and applications," *Nano Research*, vol. 1, pp. 99-115,

- 2008.
- [5] M. Vallet-Regi, A. Rámila, R. P. del Real, and J. Pérez-Pariente, "A New Property of MCM-41: Drug Delivery System," *Chemistry of Materials*, vol. 13, pp. 308-311, 2001.
- [6] C. N. Wu, T. S. Tsai, C. N. Liao, and K. J. Chao, "Controlling pore size distributions of MCM-41 by direct synthesis," *Microporous Materials*, vol. 7, pp. 173-185, 1996.
- [7] X. Li, X. Xu, Y. He, Y. Jiang, Y. Teng, Q. Wang, *et al.*, "Titanium-containing desilicated MCM-41 with bimodal pore system as green epoxidation catalyst," *Materials Letters*, vol. 146, pp. 84-86, 2015.
- [8] I. Ushiki, M. Ota, Y. Sato, and H. Inomata, "VOCs (acetone, toluene, and n-hexane) adsorption equilibria on mesoporous silica (MCM-41) over a wide range of supercritical carbon dioxide conditions: Experimental and theoretical approach by the Dubinin–Astakhov equation," *Fluid Phase Equilibria*, vol. 403, pp. 78-84, 2015.
- [9] Y. Ma, S. Qing, D. Yin, X. Mamat, J. Zhang, Z. Gao, *et al.*, "Rh-based catalysts supported on MCM-41-type mesoporous silica for dicyclopentadiene hydroformylation," *Catalysis Today*, 2015.
- [10] S. Shen, J. Chen, R. T. Koodali, Y. Hu, Q. Xiao, J. Zhou, *et al.*, "Activation of MCM-41 mesoporous silica by transition-metal incorporation for photocatalytic hydrogen production," *Applied Catalysis B: Environmental*, vol. 150-151, pp. 138-146, 2014.
- [11] H. I. Meléndez-Ortiz, Y. Perera-Mercado, J. A. Mercado-Silva, Y. Olivares-Maldonado, G. Castruita, and L. A. García-Cerda, "Functionalization with amine-containing organosilane of mesoporous silica MCM-41 and MCM-48 obtained at room temperature," *Ceramics International*, vol. 40, pp. 9701-9707, 2014.
- [12] S. Kiatphuengporn, M. Chareonpanich, and J. Limtrakul, "Effect of unimodal and bimodal MCM-41 mesoporous silica supports on activity of Fe–Cu catalysts for CO<sub>2</sub> hydrogenation," *Chemical Engineering Journal*, vol. 240, pp. 527-533, 2014.
- [13] X. Wang, Q. Guo, and T. Kong, "Tetraethylenepentamine-modified MCM-41/silica gel with hierarchical mesoporous structure for CO<sub>2</sub> capture," *Chemical Engineering Journal*, vol. 273, pp. 472-480, 2015.
- [14] F. Farjadian, P. Ahmadpour, S. M. Samani, and M. Hosseini, "Controlled size synthesis and application of nanosphere MCM-41 as potent adsorber of drugs: A novel approach to new antidote agent for intoxication," *Microporous and Mesoporous Materials*, vol. 213, pp. 30-39, 2015.
- [15] J. B. Raoof, F. Chekin, and V. Ehsani, "Palladium-doped mesoporous silica SBA-15 modified in carbon-paste electrode as a sensitive voltammetric sensor for detection of oxalic acid," *Sensors and Actuators B: Chemical*, vol. 207, pp. 291-296, 2015.
- [16] L. Laskowski and M. Laskowska, "Functionalization of SBA-15 mesoporous silica by Cu-phosphonate units: Probing of synthesis route," *Journal of Solid State Chemistry*, vol. 220, pp. 221-226, 2014.
- [17] S. Wang, K. Wang, C. Dai, H. Shi, and J. Li, "Adsorption of Pb<sup>2+</sup> on amino-functionalized core–shell magnetic mesoporous SBA-15 silica composite," *Chemical Engineering Journal*, vol. 262, pp. 897-903, 2015.
- [18] N. R. Srinivasan, P. Majumdar, N. K. R. Eswar, and R. Bandyopadhyaya, "Photocatalysis by morphologically tailored mesoporous silica (SBA-15)

- embedded with SnO<sub>2</sub> nanoparticles: Experiments and model," *Applied Catalysis A: General*, vol. 498, pp. 107-116, 2015.
- [19] J. H. Yang, Y.-J. Cho, J. M. Shin, and M.-S. Yim, "Bismuth-embedded SBA-15 mesoporous silica for radioactive iodine capture and stable storage," *Journal of Nuclear Materials*, vol. 465, pp. 556-564, 2015.
- [20] W. Xie, X. Yang, and M. Fan, "Novel solid base catalyst for biodiesel production: Mesoporous SBA-15 silica immobilized with 1,3-dicyclohexyl-2-octylguanidine," *Renewable Energy*, vol. 80, pp. 230-237, 2015.
- [21] M. M. Wan, X. D. Sun, S. Liu, J. Ma, and J. H. Zhu, "Versatile drug releaser derived from the Ti-substituted mesoporous silica SBA-15," *Microporous and Mesoporous Materials*, vol. 199, pp. 40-49, 2014.
- [22] J. R. Matos, L. P. Mercuri, M. Kruk, and M. Jaroniec, "Toward the Synthesis of Extra-Large-Pore MCM-41 Analogues," *Chemistry of Materials*, vol. 13, pp. 1726-1731, 2001.
- [23] M. M. Wan, J. Y. Yang, Y. Qiu, Y. Zhou, C. X. Guan, Q. Hou, *et al.*, "Sustained Release of Heparin on Enlarged-Pore and Functionalized MCM-41," *ACS Applied Materials & Interfaces*, vol. 4, pp. 4113-4122, 2012.
- [24] S. Loganathan, M. Tikmani, and A. K. Ghoshal, "Novel Pore-Expanded MCM-41 for CO<sub>2</sub> Capture: Synthesis and Characterization," *Langmuir*, vol. 29, pp. 3491-3499, 2013.
- [25] A. Sayari, P. Liu, M. Kruk, and M. Jaroniec, "Characterization of Large-Pore MCM-41 Molecular Sieves Obtained via Hydrothermal Restructuring," *Chemistry of Materials*, vol. 9, pp. 2499-2506, 1997.
- [26] S. Namba, a. Mochizuki, and M. Kito, "Preparation of highly ordered MCM-41 with docosyltrimethylammonium chloride (C<sub>22</sub>TMAC1) as a template and fine control of its pore size," *Stud Surf Sci Catal*, vol. 117, pp. 257-264, 1998.
- [27] I. Diaz, J. Pérez-Pariente, and E. Sastre, "Porous materials in environmentally friendly processes, Proceedings of the 1st international FEZA conference," *Studies in Surface Science and Catalysis*, vol. 125, pp. 53-60, 1999.
- [28] X. Wang, K. S. K. Lin, J. C. C. Chan, and S. Cheng, "Direct Synthesis and Catalytic Applications of Ordered Large Pore Aminopropyl-Functionalized SBA-15 Mesoporous Materials," *The Journal of Physical Chemistry B*, vol. 109, pp. 1763-1769, 2005.
- [29] M. Kruk and L. Cao, "Pore Size Tailoring in Large-Pore SBA-15 Silica Synthesized in the Presence of Hexane," *Langmuir*, vol. 23, pp. 7247-7254, 2007.
- [30] Y. Kang, J. He, X. GuoGuo, Guo, and Z. Song, "Influence of Pore Diameters on the Immobilization of Lipase in SBA-15," *Industrial & Engineering Chemistry Research*, vol. 46, pp. 4474-4479, 2007.
- [31] L. Cao, T. Man, and M. Kruk, "Synthesis of Ultra-Large-Pore SBA-15 Silica with Two-Dimensional Hexagonal Structure Using Triisopropylbenzene As Micelle Expander," *Chemistry of Materials*, vol. 21, pp. 1144-1153, 2009.
- [32] S. Wu, W. Zhang, S. Jia, Y. Liu, J. Ran, H. Ren, *et al.*, "Novel pathway for the synthesis of monodisperse MCM-41 nanospheres with different particle size distributions," *Materials Letters*, vol. 98, pp. 138-141, 2013.
- [33] S. Lim, A. Ranade, G. Du, L. D. Pfefferle, and G. L. Haller, "Pseudomorphic Synthesis of Large-Particle Co-MCM-41," *Chemistry of*

- Materials*, vol. 18, pp. 5584-5590, 2006.
- [34] M. Varache, I. Bezverkhyy, L. Saviot, F. Bouyer, F. Baras, and F. Bouyer, "Optimization of MCM-41 type silica nanoparticles for biological applications: Control of size and absence of aggregation and cell cytotoxicity," *Journal of Non-Crystalline Solids*, vol. 408, pp. 87-97, 2015.
- [35] X. Liu, H. Sun, Y. Chen, Y. Yang, and A. Borgna, "Preparation of spherical large-particle MCM-41 with a broad particle-size distribution by a modified pseudomorphic transformation," *Microporous and Mesoporous Materials*, vol. 121, pp. 73-78, 2009.
- [36] A.-M. Hanu, S. Liu, V. Meynen, P. Cool, E. Popovici, and E. F. Vansant, "Influence of the MCM-41 morphology on the vanadia deposition by a molecular designed dispersion method," *Microporous and Mesoporous Materials*, vol. 95, pp. 31-38, 2006.
- [37] Q. Qu, G. Zhou, Y. Ding, S. Feng, and Z. Gu, "Adjustment of the morphology of MCM-41 silica in basic solution," *Journal of Non-Crystalline Solids*, vol. 405, pp. 104-115, 2014.
- [38] A. I. Carrillo, E. Serrano, R. Luque, and J. García-Martínez, "Microwave-assisted catalysis by iron oxide nanoparticles on MCM-41: Effect of the support morphology," *Applied Catalysis A: General*, vol. 453, pp. 383-390, 2013.
- [39] S. Jana, B. Dutta, H. Honda, and S. Koner, "Mesoporous silica MCM-41 with rod-shaped morphology: Synthesis and characterization," *Applied Clay Science*, vol. 54, pp. 138-143, 2011.
- [40] A. Carrero, J. Moreno, J. Aguado, and G. Calleja, "Zeolites and related materials: Trends, targets and challenges, Proceedings of the 4th International FEZA Conference," *Studies in Surface Science and Catalysis*, vol. 174, pp. 321-324, 2008.
- [41] E. M. Johansson, J. M. Córdoba, and M. Odén, "The effects on pore size and particle morphology of heptane additions to the synthesis of mesoporous silica SBA-15," *Microporous and Mesoporous Materials*, vol. 133, pp. 66-74, 2010.
- [42] S. Saravanamurugan, D.-S. Han, J.-B. Koo, and S.-E. Park, "Transesterification reactions over morphology controlled amino-functionalized SBA-15 catalysts," *Catalysis Communications*, vol. 9, pp. 158-163, 2008.
- [43] N. Osakoo, R. Henkel, S. Loiha, F. Roessner, and J. Wittayakun, "Effect of support morphology and Pd promoter on Co/SBA-15 for Fischer-Tropsch Synthesis," *Catalysis Communications*, vol. 56, pp. 168-173, 2014.
- [44] Q. Cai, W.-y. Lin, F.-s. Xiao, W.-q. Pang, X.-h. Chen, and B.-s. Zou, "The preparation of highly ordered MCM-41 with extremely low surfactant concentration," vol. 32, pp. 1-15, 1999.
- [45] S.-M. Lai, H.-Y. Lai, and M.-Y. Chou, "A facile approach for the tunable wormlike or ordered pore morphology of mesoporous silica: Effect of catalyst types and polyethylene glycol," *Microporous and Mesoporous Materials*, vol. 196, pp. 31-40, 2014.
- [46] Z. AlOthman, "A Review: Fundamental Aspects of Silicate Mesoporous Materials," *Materials*, vol. 5, pp. 2874-2902, 2012.

## اثر شرایط سنتز بر خواص بافتی سیلیکا MCM-41

سید عباس سجادی<sup>۱</sup>، علی ایزدبخش<sup>۱\*</sup>، خدابخش نیکنام<sup>۲</sup>

۱. گروه مهندسی شیمی، دانشکده مهندسی نفت، گاز و پتروشیمی، دانشگاه خلیج فارس، بوشهر، ایران

۲. گروه شیمی، دانشکده علوم پایه، دانشگاه خلیج فارس، بوشهر، ایران

### مشخصات مقاله

تاریخچه مقاله:

دریافت: ۳۱ فروردین ۱۳۹۵

پذیرش نهایی: ۱۸ آبان ۱۳۹۵

کلمات کلیدی:

MCM-41

مزوحفره

نانو

سل ژل

سیلیکا

\* عهده‌دار مکاتبات؛

رایانامه: izadbaksh@pgu.ac.ir

تلفن: +۹۸ ۹۱۲ ۵۴۳۱۳۵۱

دورنگار: +۹۸ ۷۷ ۳۳۴۴۱۴۹۵

### چکیده

نمونه‌های مختلف سیلیکای مزوحفره با روش سل ژل در حضور قالب‌ساز CTAB با تغییر شدت همزدگی و زمان هضم، نسبت CTAB به سیلیکا و آمونیوم هیدروکسید به آب در مخلوط سنتز تهیه شدند. همچنین اثر دمای هضم، دمای عملیات آبی-گرمایی و افزودن ترشری بوتانول بر خواص بافت نمونه‌های حاصل مورد مطالعه قرار گرفت. نتایج XRD، SEM و آزمون جذب همدمای N<sub>2</sub> نشان داد که شرایط سنتز اندازه ذرات و شکل سیلیکای مزوحفره منظم را تحت تأثیر قرار می‌دهد، اگر چه تغییرات اندازه حفره ( $< 5 \text{ \AA}$ ) قابل توجه نبود. اثر دما بر اندازه حفره، سلول واحد و شکل ذرات نمونه‌های سنتزی از عوامل دیگر مؤثرتر مشخص شد. همچنین نتایج نشان داد تغییرات عمده ظاهری ذرات نمونه‌های سنتزی شامل تغییر (شکل کروی به ذرات بزرگتر کرمی شکل)، بلورینگی و شدت توده‌ای شدن می‌باشد. نمونه‌های MCM-41 در محدوده اندازه ۵۰ nm تا ۱  $\mu\text{m}$  با کاهش دمای هضم به دست آمد. عملیات آبی-گرمایی به تشکیل ذرات شش وجهی با اندازه ۵۰۰ nm منجر گردید. در حالی که افزایش شدت همزدگی موجب کاهش اندازه ذرات گردید، با افزودن ترشری بوتانول به مخلوط سنتز ذرات کرم مانند MCM-41 تا طول ۲  $\mu\text{m}$  به دست آمد.